INTERNATIONAL CENTER FOR NUMERICAL METHODS IN ENGINEERING

A General Methodology for Deriving Shear Contrained Reissner Mindlin Plate Elements

E. Oñate
O. C. Zienkiewicz
B. Suárez
R. L. Taylor

Publication, CIMNE Nº 5, 1990

A General Methodology for Deriving Shear Contrained Reissner Mindlin Plate Elements

E. Oñate
O. C. Zienkiewicz
B. Suárez
R. L. Taylor

Submited for publication to the International Journal for Numerical Methods in Engineering

Publication CIMNE Nº-5, 1990

International Center for Numerical Methods in Engineering
Gran Capitán s/n, 08034 Barcelona, Spain

A GENERAL METHODOLOGY FOR DERIVING SHEAR CONSTRAINED REISSNER–MINDLIN PLATE ELEMENTS

E. OÑATE*, O.C. ZIENKIEWICZ***, B. SUAREZ* and R.L. TAYLOR**

*Universidad Politécnica de Catalunya, 08039 Barcelona, Spain.
**University of California, Berkeley, U.S.A.
***University College of Swansea, U.K.

Summary

In this paper the necessary requirements for the good behaviour of shear constrained Reissner-Mindlin plate elements for thick and thin plate situations are re-interpreted and a simple explicit form of the substitute shear strain matrix is obtained. This extends the previous work of the authors presented in [20], [19].The general methology is applied to the re-formulation of some well known quadrilateral plate elements and some new triangular and quadrilateral plate elements which show promising features. Some examples of the good behaviour of these elements are given.

1. INTRODUCTION

Recent work in the development of efficient plate finite elements has been mostly based in the so called Reissner-Mindlin thick plate theory [14],[17]. This by-passes the difficulties caused by the C^1 requirement of the classic Kirchhoff theory [18], [20]. However, its direct aplications to thin plate situations can induce locking and various artifices to eliminate this effect, like the introduction *of reduced or selective integration* procedures [1],[11], [12],[16],[19], [22] or the use of *constrained substitute shear strain fields* [2]–[4], [7]–[10], [15], [21], [24] have been proposed.

It is now clear that both these approaches can been re-interpreted in the more general framework of a mixed formulation in which shear forces and displacements are approximated independently [20]. Moreover, the mixed form provides the necessary requirements that the elements should satisfy to be applicable for both thick and thin plate situations . This has allowed to define a general methodology for the formulation of successful shear constrained plate elements [15] and some of these have been recently reported by the autors [15], [21].

In this paper we re-examine the problem of thick plate elements based on constrained shear strain fields. We show that the condition of vanishing shear strain for the thin plate limit can only be naturally achieved if the coefficients defining the approximating shear strain polynomial are a linear function of both nodal rotations and deflections. This explains the success of reduced integration techniques and the use of constrained transverse shear strain fields which lead to the satisfaction of such

a condition. In the paper, the methodology proposed in [15] for defining "a priori" adequate constrained shear strain fields and for the derivation of the corresponding substitute shear strain matrix is detailed. This methodology is applied to re-formulate the well known 4 and 9 node quadrilateral plate elements of Bathe and Dvorkin [3],[9] and Hinton and Huang [10], the new triangular elements of Zienkiewicz et al [24] and some new quadrilateral and triangular elements. Finally, examples of the good behaviour of these elements is given.

2. BASIC CONCEPTS

The basic expressions of the Reissner-Mindlin plate theory are the following:

Plate curvatures

$$\boldsymbol{\chi} = \begin{Bmatrix} \chi_x \\ \chi_y \\ \chi_{xy} \end{Bmatrix} = \begin{Bmatrix} \frac{\partial \theta x}{\partial x} \\ \frac{\partial \theta y}{\partial y} \\ \frac{\partial \theta x}{\partial y} + \frac{\partial \theta y}{\partial x} \end{Bmatrix} = \begin{bmatrix} \frac{\partial}{\partial x} & 0 \\ 0 & \frac{\partial}{\partial y} \\ \frac{\partial}{\partial y} & \frac{\partial}{\partial x} \end{bmatrix} \begin{Bmatrix} \theta_x \\ \theta_y \end{Bmatrix} = \mathbf{L}\ \boldsymbol{\theta} \qquad (1)$$

Shear strains

$$\boldsymbol{\gamma} = \begin{Bmatrix} \gamma_x \\ \gamma_y \end{Bmatrix} = \begin{Bmatrix} \frac{\partial w}{\partial x} + \theta_x \\ \frac{\partial w}{\partial y} + \theta_y \end{Bmatrix} = \begin{bmatrix} \frac{\partial}{\partial x} & 1 & 0 \\ \frac{\partial}{\partial y} & 0 & 1 \end{bmatrix} \begin{Bmatrix} w \\ \theta_x \\ \theta_y \end{Bmatrix} = \mathbf{S}\ \mathbf{u} \qquad (2)$$

In above w, θ_x and θ_y are the deflection and rotations of a point in the plate mid-surface. For sign convenion see Figure 1.

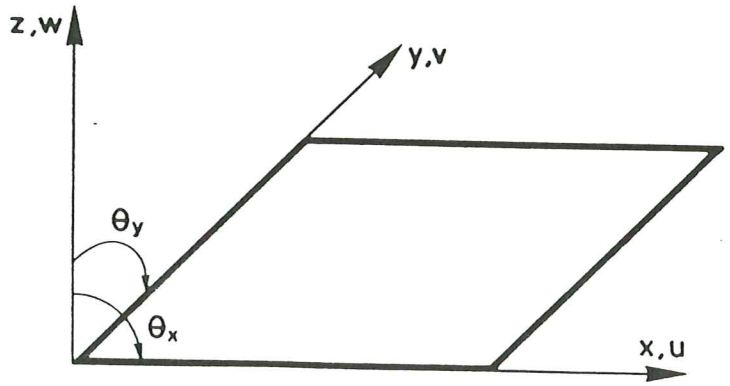

Figure 1. Definition of displacement variables in a plate.

Bending moments/curvature relationship (isotropic conditions only presented)

$$\mathbf{m} = \begin{Bmatrix} M_x \\ M_y \\ M_{xy} \end{Bmatrix} = \frac{Et^3}{12(1-\nu^2)} \begin{bmatrix} 1 & \nu & 0 \\ \nu & 1 & 0 \\ 0 & 0 & \frac{1-\nu}{2} \end{bmatrix} \begin{Bmatrix} \chi_x \\ \chi_y \\ \chi_{xy} \end{Bmatrix} = \mathbf{D}_b \ \boldsymbol{\chi} \tag{3}$$

Shear forces/shear strains relationship

$$\mathbf{s} = \begin{Bmatrix} Q_x \\ Q_y \end{Bmatrix} = G\alpha t \begin{bmatrix} 1 & 0 \\ 0 & 1 \end{bmatrix} \begin{Bmatrix} \gamma_x \\ \gamma_y \end{Bmatrix} = \mathbf{D}_s \ \boldsymbol{\gamma} \tag{4}$$

In above E, G, ν ,t are the Young's modulus, shear modulus, the Poisson's ratio and the plate thickness, respectively and α is the warping coefficient accounting for non uniform shear distribution (usually taken as $\alpha = 5/6$).

Total plate energy

$$\Pi = \frac{1}{2}\int\int_A \boldsymbol{\chi}^T \mathbf{m} \, dA + \frac{1}{2}\int\int_A \boldsymbol{\gamma}^T \mathbf{s} \, dA - \int\int_A wq \, dA \tag{5}$$

The first two integrals of (5) represent the bending and shear energies, respectively, whereas the third one represents the external energy due to a distributed force q acting over the plate area A.

3. FINITE ELEMENT DISCRETIZATION

Consider a finite element discretization of the plate using isoparametric elements [19]. The deflection w and the rotations θ_x, θ_y can be interpolated using a different approximation as

$$w = \mathbf{N}_w \bar{\boldsymbol{w}} \quad , \quad \boldsymbol{\theta} = \mathbf{N}_\theta \bar{\boldsymbol{\theta}} \tag{6}$$

where $(\bar{\cdot})$ denotes nodal (or internal parameters) values ($\bar{\boldsymbol{w}}_i = [w_i]$, $\bar{\boldsymbol{\theta}}_i = [\theta_{x_i}, \theta_{y_i}]^T$).

Eqs.(6) can be combined to give

$$\mathbf{u} = [w, \theta_x, \theta_y]^T = \mathbf{N}\bar{\mathbf{u}} \tag{7}$$

$$\text{with } \bar{\mathbf{u}}_i = [w_i, \theta_{x_i}, \theta_{y_i}]^T \ , \ \mathbf{N}_i = \begin{bmatrix} N_{w_i} & \\ & \mathbf{N}_{\theta_i} \end{bmatrix} \ , \ \mathbf{N}_{\theta_i} = N_{\theta_i}\mathbf{I}_2 \tag{8}$$

where N_{w_i} and N_{θ_i} are the C^0 shape functions interpolating the deflections and the rotations, respectively.

Substitution of eqs.(6)–(7) in (1)–(2) yields

$$\boldsymbol{\chi} = \mathbf{L}\boldsymbol{\theta} = \mathbf{L}\mathbf{N}_\theta\bar{\boldsymbol{\theta}} = \mathbf{B}_b\bar{\mathbf{u}} \tag{9}$$

$$\boldsymbol{\gamma} = \mathbf{S}\mathbf{u} = \mathbf{S}\mathbf{N}\bar{\mathbf{u}} = \mathbf{B}_s\bar{\mathbf{u}} \tag{10}$$

where $\mathbf{B}_b$ and $\mathbf{B}_s$ are the standard bending and shear strain matrices, respectively given by

$$\mathbf{B}_b = \begin{bmatrix} 0 & \frac{\partial N_i^\theta}{\partial x} & 0 \\ 0 & 0 & \frac{\partial N_i^\theta}{\partial y} \\ 0 & \frac{\partial N_i^\theta}{\partial y} & \frac{\partial N_i^\theta}{\partial x} \end{bmatrix} \quad ; \quad \mathbf{B}_s = \begin{bmatrix} \frac{\partial N_i^w}{\partial x} & N_i^\theta & 0 \\ \frac{\partial N_i^w}{\partial y} & 0 & N_i^\theta \end{bmatrix} \tag{11}$$

Substitution of eqs.(9)–(10) in the expression of the potential energy (5) yields, after minimization, the discretized equilibrium expressions and the usual form of the bending and shear stiffness matrices is obtained as [10],[16].

$$\mathbf{K}^{(e)} = \mathbf{K}_b^{(e)} + \mathbf{K}_s^{(e)} \tag{12}$$

with

$$\mathbf{K}_b^{(e)} = \int\int_{A^{(e)}} \mathbf{B}_b^T\mathbf{D}_b\mathbf{B}_b dA \quad ; \quad \mathbf{K}_s^{(e)} = \int\int_{A^{(e)}} \mathbf{B}_s^T\mathbf{D}_s\mathbf{B}_s dA \tag{13}$$

where, indexes b and s refer to bending and shear contributions, respectively.

4. THIN PLATE LIMIT

In the thin plate limit Kirchhoff's assumptions of vanishing transverse shear strain must be satisfied. This implies $\boldsymbol{\gamma} = \mathbf{0}$. From eq.(10) we can write for rectangular or straight sides triangular elements with n nodes

$$\boldsymbol{\gamma} = \mathbf{B}_s\bar{\mathbf{u}} = \boldsymbol{\alpha}_1(\bar{\omega},\bar{\theta}) + \boldsymbol{\alpha}_2(\bar{\omega},\bar{\theta})\xi + \boldsymbol{\alpha}_3(\bar{\omega},\bar{\theta})\eta + \cdots + \boldsymbol{\alpha}_n(\bar{\omega},\bar{\theta})\xi^p\eta^q = 0 \tag{14}$$

Satisfaction of (14) implies of course that

$$\boldsymbol{\alpha}_j(\bar{\omega},\bar{\boldsymbol{\theta}}) = 0 \quad ; \quad j = 1,n \tag{15}$$

Eq.(15) imposes a set of linear relationships between nodal deflections and rotations which usually can also be interpreted on physical grounds. Only elements satisfying (15) indentically can, in the limit, reproduce naturally the thin plate conditions with absence of locking.

However, in many elements the α_j's are a function of the nodal rotations only, and the condition $\alpha_j(\theta_i) = 0$, requiring that $\theta_i = 0$ for the thin plate solution, prevents any bending strains and hence leads to locking.

The above concepts will be applied to two well know beam and plate elements in next section.

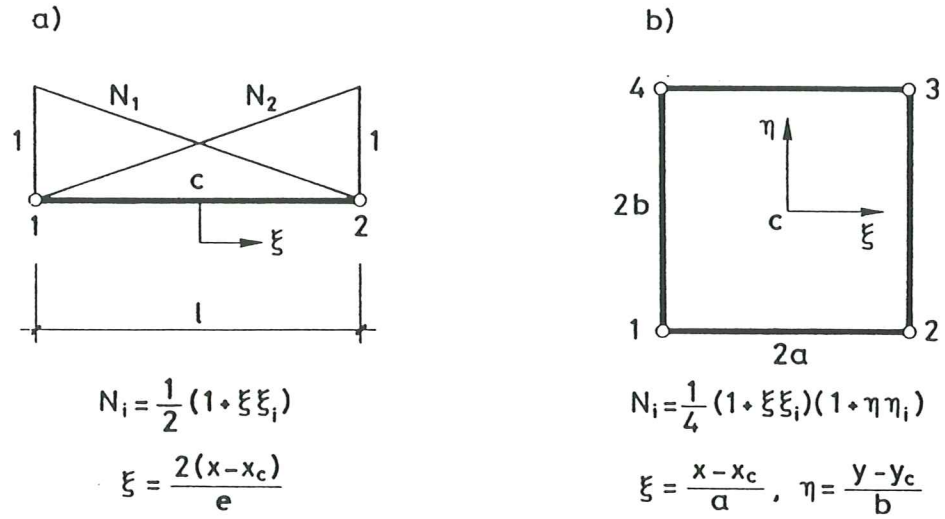

Figure 2. (a) Two node linear Timoshenko beam element. (b) Four node rectangular plate element.

4.1. Two node linear Timoshenko beam element

The geometry of the element is shown in Figure 2a. The displacement field is interpolated as

$$w = \sum_{i=1}^{2} N_i w_i \quad , \quad \theta = \sum_{i=1}^{2} N_i \theta_i \tag{16}$$

The one dimensional shape functions $N_i(\xi)$ are also shown in Figure 2. The shear strain field is obtained as

$$\gamma = \frac{\partial w}{\partial x} + \theta = \left[\frac{w_2 - w_2}{\ell} + \frac{\theta_1 + \theta_2}{2}\right] + \frac{1}{2}(\theta_2 - \theta_1)\xi = \\ = \alpha_1(w_i, \theta_i) + \alpha_2(\theta_i)\xi \tag{17}$$

The Euler-Bernoulli condition ($\gamma = 0$), implies

$$\gamma = 0 \Longrightarrow \begin{cases} \alpha_1 = 0 \quad i.e. \quad \frac{w_1 - w_2}{\ell} = \frac{\theta_1 + \theta_2}{2} \\ \alpha_2 = 0 \quad i.e. \quad \theta_1 = \theta_2 \end{cases} \tag{18}$$

The condition on α_1 physically means that the average element rotation equals the element slope, which is clearly satisfied for slender beams. On the other hand, $\alpha_2 = 0$ imposes an uniform or zero rotation on the element. This invariably leads to a vanishing of the bending energy and thus to locking.

4.2 Four node rectangular Reissner-Mindlin plate element

The element geometry is shown in Figure 2b. The displacement field is given by

$$w = \sum_{i=1}^{4} N_i w_i \quad , \quad \boldsymbol{\theta} = [\theta_x, \theta_y]^T = \sum_{i=1}^{4} N_i \boldsymbol{\theta}_i \tag{19}$$

Where the bilinear shape functions N_i are also shown in Figure 2.
Lets's consider the expression of the transverse shear strain γ_x

$$\begin{aligned} \gamma_x = \frac{\partial w}{\partial x} + \theta_x = \sum_{i=1}^{4} \Big[(\frac{\xi_i}{4a} w_i + \frac{1}{4}\theta_{x_i}) + (\frac{\xi_i \eta_i}{4a} w_i + \frac{\eta_i}{4}\theta_{x_i})\eta + \\ (\frac{\xi_i}{4}\theta_{x_i})\xi + (\frac{\xi_i \eta_i}{4}\theta_{x_i})\xi\eta \Big] = \alpha_1(w_i, \theta_{x_i}) + \\ + \alpha_2(w_i, \theta_{x_i})\eta + \alpha_3(\theta_{x_i})\xi + \alpha_4(\theta_{x_i})\xi\eta \end{aligned} \tag{20}$$

A similar expression can be obtained for γ_y simply interchanging x and ξ by y and η.

The limiting Kirchhoff conditions ($\gamma_x = \gamma_y = 0$) implie now $\alpha_1 = \alpha_2 = \alpha_3 = \alpha_4 = 0$. Clearly the conditions on α_1 and α_2 impose a linear relationship between the nodal deflections and the average θ_x rotation (θ_y for γ_y) on the element. This can be physically interpreted similarly as in the case of the condition $\alpha_1 = 0$ for the beam element of previous example. However, the element is unable to satisfy naturaly the conditions $\alpha_3 = \alpha_4 = 0$, and this leads to the trivial solution $\theta_{x_i} = 0$ ($\theta_{y_i} = 0$ for γ_y) and thus to locking.

4.3 Some remedies to avoid locking

From these examples it can be deduced that a simple way to avoid locking is to evaluate the shear strains only in points where the spurious $\alpha_k(\theta_i)$ vanish, using for instance a numerical quadrature based on such points. Thus, for the two node beam element computation of γ at the element mid-point eliminates the undesirable α_2 coefficient leading to

$$[\gamma]_{\xi=0} = \alpha_1 = \left[\frac{w_2 - w_1}{\ell} + \frac{\theta_1 + \theta_2}{2}\right] = \left[-\frac{1}{\ell}, \frac{1}{2}, \frac{1}{\ell}, \frac{1}{2}\right]\bar{\mathbf{u}} = \hat{\mathbf{B}}_s\bar{\mathbf{u}} \quad (21)$$

Matrix $\hat{\mathbf{B}}_s$ is termed in literature "substitute shear strain matrix" [10], [12]. Computation of the element stiffness matrix simply implies now to use $\hat{\mathbf{B}}_s$ instead of the standard shear strain matrix $\mathbf{B}_s$ in the computation of $\mathbf{K}_s^{(e)}$, while the bending contribution $\mathbf{K}_b^{(e)}$ remains unaltered (eq.(13)).

For the four node rectangular plate element we observe that the spurious coefficients α_3 and α_4 vanish automatically if γ_x is sampled on quadrature points along the line $\xi = 0$ (conversely γ_y should be sampled along the line $\eta = 0$). The derivation of the resulting $\hat{\mathbf{B}}_s$ matrix for this case is obvious and can use either the standard single point quadrature for γ_x and γ_y of $\xi = \eta = 0$, or alternatively 2 points for γ_x and two separate points for γ_y.

The preceeding arguments are the basis of the well known reduced integration procedures widely used in practice [1], [11], [13], [16], [19], [22]. However, reduced integration techniques have proved not to be generally sufficient for the development of robust isoparametric thick plate elements, leading frequently to mechanisms which can polute the solution [11], [12], [19], [22]. An alternative procedure is to impose "a priori" a shear strain field which satisfies condition (15), thus allowing the natural satisfaction of the limit thin plate condition. The shear strains are now written as

$$\boldsymbol{\gamma} = \sum_{k=1}^{m} \mathbf{N}_{\gamma_k}\,\boldsymbol{\gamma}_k = \mathbf{N}_\gamma\,\bar{\boldsymbol{\gamma}} \quad (22)$$

Where $\boldsymbol{\gamma}_k$ are the values of the shear strains at some selected points within the element. Combining eqs.(16) and (10) yields

$$\boldsymbol{\gamma} = \sum_{k=1}^{m} \mathbf{N}_{\gamma_k}\mathbf{B}_{s_k}\mathbf{u}_k = \hat{\mathbf{B}}_s\bar{\mathbf{u}} \quad (23)$$

It is easy to choose eq.(22) so that eq.(15) is satisfied to guarantee the absence of locking.

The spproximation to the total potential energy can now be written using eqs.(9) and (22) as

$$\Pi = \frac{1}{2}\int\int_A [\mathbf{L}\boldsymbol{\theta}]^T \mathbf{D}_b \mathbf{L}\boldsymbol{\theta}\, dA + \frac{1}{2}\int\int_A [\mathbf{N}_\gamma\, \bar{\boldsymbol{\gamma}}]^T \mathbf{D}_s \mathbf{N}_\gamma\, \bar{\boldsymbol{\gamma}}\, dA - \int\int_A wq\, dA \quad (24)$$

Above expression can be used for generation of stiffness equations written in terms of **u** only when constraints relating **u** and $\boldsymbol{\gamma}$ have been imposed (eqs.(2) or (3)). In the next section we shall discuses how such constraints are imposed Note that in (24) C^0 continuity is required for the rotations $\boldsymbol{\theta}$, whereas the deflection w, and the substitute shear strains $\bar{\gamma}$ can be discontinuous. This possibility has been exploted by Arnold and Falk in the development of a three node triangular plate element with a discontinuous deflection field [2].

5. CHOICE OF SUBSTITUTE STRAIN FIELDS

Adequate substitute strain fields can be successfully chosen by direct observation, having in mind the objectives of obtaining strain fields satisfying eq.(15).

Thus, from the expression of γ for the 2D linear beam element (eq.(17)) it is easy to define a constant substitute strain field as

$$\gamma = \alpha_1(w_i, \theta_i) \quad (25)$$

The value of α_1 can be obtained by sampling γ at the element mid point. Thus in effect achieving the constraint of eq.(2) by collocation at that point. This leads to an identical expression for the substitute shear strain matrix to that given in eq.(21) using one point selective integration. The analogy between both procedures becomes quite evident in this case.

For the bilinear rectangular plate element we can write after observation of the initial strain field (see (eq.(20))

$$\begin{aligned} \gamma_x &= \alpha_1(w_i, \theta_{x_i}) + \alpha_2(w_i, \theta_{x_i})\eta \\ \gamma_y &= \alpha_3(w_i, \theta_{y_i}) + \alpha_4(w_i, \theta_{y_i})\xi \end{aligned} \quad (26)$$

The values of the α_i's can be computed by sampling the shear strains (or colocating eq.(2)) at the four points shown in Figure 3a and the substitutive shear strain matrix can be readily obtained. The reader will inmediately recognize this element to be identical to that proposed by Bathe and Dvorkin [3],[9].

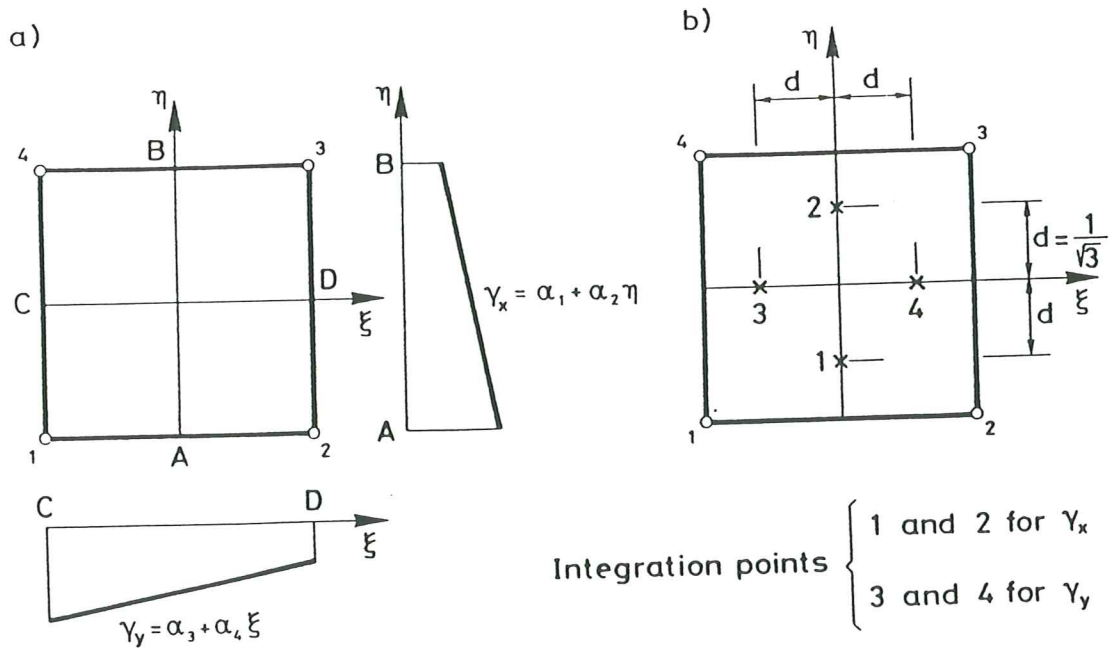

Figure 3. Four node quadrilateral plate element: (a) Assumed shear strain field. (b) Integration points for the γ_x and γ_y terms in the original shear stiffness matrix.

It is interesting to note that the shear stiffness matrix for this case using exact (2×2) integration is identical to that obtained with the original shear strain field and the four points selective quadrature rule shown in Figure 3b.

The reason for this is that:

(1) A collocation of the initial shear strain field (viz eq.(10)) along the lines $\xi = 0$ and $\eta = 0$ for γ_x and γ_y respectively yields *precisely* the strain field of eq.(26).

2) The two points quadrature along the lines $\xi = 0$ and $\eta = 0$ for the original γ_x and γ_y terms, respectively (Figure 3b), integrate *exactly* the quadratic terms in η and ξ contained in the shear stiffness matrix, thus yielding the some final expresssion for $\mathbf{K}_s$ as that directly obtained from eq.(26).

For a general quadrilateral with isoparametric coordinates ξ and η the situation is identical as for as the first point above is concerned providing γ_ξ and γ_η are used instead of γ_x and γ_y. However the two Gauss point integration of Figure 3b is no longer exact and yields a different shear stiffness matrix (and worst numerical results) than that obtained using a 2×2 integration.

We would indeed anticipate the element to give very similar results (and to have some difficiences) if a single point quadrature were used for the shear terms in the manner originally suggested by Hughes et al [11].

It has been shown [20],[23] that the choice of the substitute strain field must satisfy certain additional requirements if singularity and locking are to be avoided. Starting

with the mixed form in which deflections, rotations and shear strains are independently interpolated the neccesary conditions to be satisfied are

$$n_\theta + n_w \geq n_\gamma \tag{27a}$$

$$n_\gamma \geq n_w \tag{27b}$$

There n_w, n_θ and n_γ stand for the number of "free" variables (afther discounting the prescribed boundary conditions) in each set of interpolating parameters $\bar{\boldsymbol{w}}$, $\bar{\boldsymbol{\theta}}$ and $\bar{\boldsymbol{\gamma}}$, respectively.The above inequalities have to be satisfed for any element patches as a condition which is necessary (although not always sufficient) for convergence [23].

It is interesting to note that the inequality (27a) can also be interpreted as a generalization of the well known "singularity rule" widely used in the context of reduced integration techniques to define approximate quadratures giving a singular shear stiffness matrix $\mathbf{K}_s$, thus preserving the existance of the correct numerical solution [16], [19], [22]. Elements satisfying (27a) have therefore a singular $\mathbf{K}_s$. This gives another evidence of the analogies between shear constraint methods and reduced integrations techniques. The proof of this interpretation is given in Appendix A.

In reference [24] the authors have examined a number of currently used plate elements and found that all those proving to be successfull in practice satisfy eqs.(27). Also in [24] the authors have proposed general new triangular plate elements which show very promising features. In the next section a general methology for the derivation of the substitute shear strain matrix for isoparametric plate elements is presented.

6. A METHODOLOGY FOR THE DERIVATION OF THE SUBSTITUTE SHEAR STRAIN MATRIX $\bar{\mathbf{B}}_s$

We consider the derivation of the substitute shear strain matrix of an isoparametric plate element of n nodes with an independent interpolation of deflections, rotations and shear strains defined by eqs.(6) and (22), and satisfying conditions (15).

Step 1. The starting point is the expression of the natural shear strains in a polynomial from using the natural coordinate system ξ, η, i.e.

$$\boldsymbol{\gamma}' = \begin{Bmatrix} \gamma_\xi \\ \gamma_\eta \end{Bmatrix} = \begin{bmatrix} 1 & \xi & \eta & \xi\eta & \cdots & \xi^p\eta^q & | & 0 & 0 & 0 & \cdots & 0 \\ 0 & 0 & 0 & 0 & \cdots & 0 & | & 1 & \xi & \eta & \cdots & \xi^r\eta^s \end{bmatrix} \begin{Bmatrix} \alpha_1 \\ \alpha_2 \\ \vdots \\ \alpha_{n_\gamma} \end{Bmatrix} = \mathbf{A}\boldsymbol{\alpha} \tag{28}$$

The cartesian shear strains are directly obtained as

$$\boldsymbol{\gamma} = \begin{Bmatrix} \gamma_x \\ \gamma_y \end{Bmatrix} = \mathbf{J}^{-1}\boldsymbol{\gamma}' \tag{29}$$

where $\mathbf{J}$ is the standard 2×2 jacobian matrix of the transformation $x, y \rightarrow \xi\ ,\ \eta$.

We also define the tangential shear strain along a particular natural direction $\bar{\xi}_i$ as

$$\gamma_{\bar{\xi}_i} = \cos\beta_i \gamma_\xi + \sin\beta_i \gamma_\eta \tag{30}$$

where β_i is the angle that the direction $\bar{\xi}$ forms with the natural ξ direction. The natural directions $\bar{\xi}_i$ over the element edges can be chosen as the direction of increasing global node numbers for the end points at each element edge.

Step 2. The tangential shear strains $\gamma_{\bar{\xi}_i}$ are sampled at n_γ selected points along natural directions $\bar{\xi}_i$. Thus, substituting eq.(30) in (28) and sampling the resulting equation at the n_γ points we obtain the following system of equations

$$\mathbf{P}(\xi_i, \eta_i, \beta_i)\boldsymbol{\alpha} \ = \ \boldsymbol{\gamma}_{\bar{\xi}} \tag{31}$$

where $\boldsymbol{\gamma}_{\bar{\xi}} = [\gamma^1_{\bar{\xi}}, \gamma^2_{\bar{\xi}}, \cdots, \gamma^{n_\gamma}_{\bar{\xi}}]^T$ contains the prescribed shear strains at the n_γ sampling points. From eq.(31) we obtain

$$\boldsymbol{\alpha} \ = \ \mathbf{P}^{-1}\boldsymbol{\gamma}_{\bar{\xi}} \tag{32}$$

Step 3. The tangential shear strains $\boldsymbol{\gamma}_{\bar{\xi}}$ are related to the natural shear strains at the n_γ sampling points by the simple transformation

$$\boldsymbol{\gamma}_{\bar{\xi}} \ = \ \mathbf{T}(\beta_i)\hat{\boldsymbol{\gamma}}' \tag{33}$$

with $\hat{\boldsymbol{\gamma}}' = [\gamma^1_\xi, \gamma^1_\eta, \gamma^2_\xi, \gamma^2_\eta \cdots, \gamma^{n_\gamma}_\xi, \gamma^{n_\gamma}_\eta]^T$.

Step 4. The natural and cartesian shear strains at the sampling points are related by

$$\hat{\boldsymbol{\gamma}}' = \begin{bmatrix} \mathbf{J}^1 & & \mathbf{0} \\ & \ddots & \\ \mathbf{0} & & \mathbf{J}^{n_\gamma} \end{bmatrix} \begin{Bmatrix} \hat{\boldsymbol{\gamma}}_1 \\ \vdots \\ \hat{\boldsymbol{\gamma}}_{n_\gamma} \end{Bmatrix} = \mathbf{C}\ \hat{\boldsymbol{\gamma}} \tag{34}$$

Where $\hat{\boldsymbol{\gamma}}_i = [\gamma^i_x\ ,\ \gamma^i_y]$ and $\mathbf{J}^i$ is the jacobian matrix at the ith sampling point.

Step 5. The cartesian shear strains at the sampling points are related to the nodal displacement by

$$\hat{\boldsymbol{\gamma}} = \left\{ \begin{array}{c} \hat{\gamma}_1 \\ \vdots \\ \hat{\gamma}_{n_\gamma} \end{array} \right\} = \left\{ \begin{array}{c} \mathbf{B}_s^1 \\ \vdots \\ \mathbf{B}_s^{n_\gamma} \end{array} \right\} \bar{\mathbf{u}} = \bar{\mathbf{B}}_s \bar{\mathbf{u}} \tag{35}$$

where $\mathbf{B}_s^i$ is the standard shear strain matrix of eq.(11) computed at the ith sampling point.

Step 6. Combining steps (28), (29), (32)–(35) we can finally obtain

$$\boldsymbol{\gamma} = \mathbf{J}^{-1}\ \mathbf{A}\ \mathbf{P}^{-1}\ \mathbf{T}\ \mathbf{C}\ \bar{\mathbf{B}}_s\ \bar{\mathbf{u}}\ =\ \hat{\mathbf{B}}_s\ \bar{\mathbf{u}} \tag{36}$$

$$\text{with} \qquad \boxed{\hat{\mathbf{B}}_s = \mathbf{J}^{-1}\ \mathbf{A}\ \mathbf{P}^{-1}\ \mathbf{T}\ \mathbf{C}\ \bar{\mathbf{B}}_s} \tag{37}$$

giving the substitute shear strain matrix.

REMARK 1

In cuadrilateral plate elements with shear collocation points along the sides the expression relating the natural shear strains with their values at the collocation point can sometimes be directly obtained as $\boldsymbol{\gamma}' = [AP^{-1}T]\hat{\boldsymbol{\gamma}}'$. This avoids the computations of matrices $\mathbf{A}$, $\mathbf{P}^{-1}$ and $\mathbf{T}$ and of the corresponding matrix product.

REMARK 2

It should be noted that point sampling is not the only way to relate the tangential natural strains with the nodal displacements. Any weighting specified along the $\bar{\xi}$ directions will suffice to achieve this. For instance we can write

$$\int_{l_{\bar{\xi}}} W \left[\gamma_{\bar{\xi}} - \frac{\partial w}{\partial \bar{\xi}} - \theta_{\bar{\xi}} \right] d\bar{\xi} = 0 \tag{38}$$

where W is an appropiate weighting function. Eq.(38) allows to directly obtain an expression relating the tangential natural strains $\gamma_{\bar{\xi}}$ and the nodal displacements (steps 3–5) as

$$\gamma_{\bar{\xi}} = [TCB]\bar{\mathbf{u}} \tag{39}$$

The substitute strain matrix is now readily obtained as

$$\hat{\mathbf{B}}_s = \mathbf{J}^{-1}\mathbf{A}\mathbf{P}^{-1}[TCB] \tag{40}$$

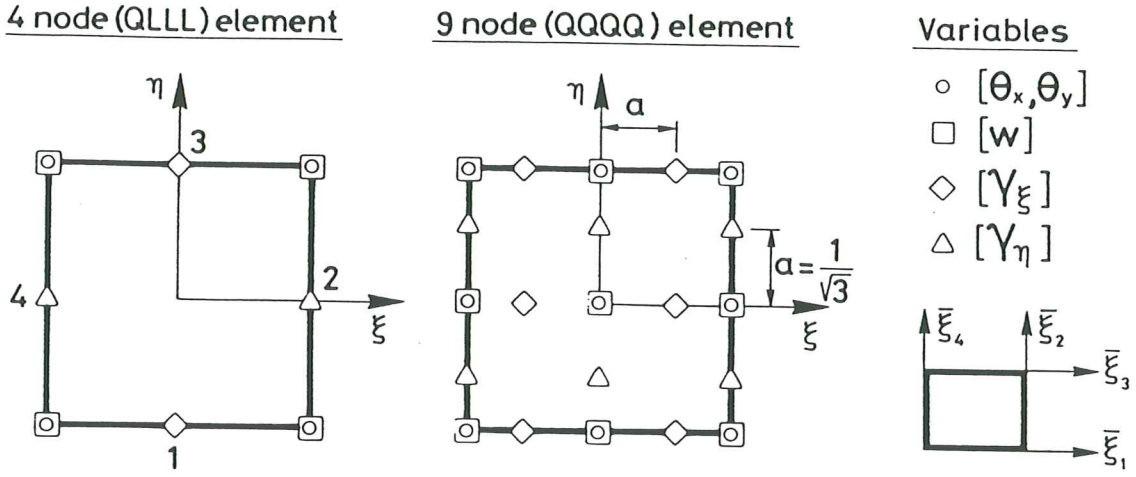

Figure 4. Four node (QLLL) and nine node (QQQQ) quadrilateral plate elements. Displacement and strain variables.

7. APPLICATIONS TO SOME OLD AND NEW PLATE ELEMENTS

7.1 Four node quadrilateral plate element with linear shear strains

The above methodology will be applied to the derivation of the substitute shear strain matrix of the well known four node plate element of Bathe and Dvorkin [3]. We choose a standard bilinear field for the interpolation of $\boldsymbol{\theta}$ and ω and the following linear shear strain field in the natural coordinate system linear

$$\begin{aligned} \gamma_\xi &= \alpha_1 + \alpha_2 \eta \\ \gamma_\eta &= \alpha_3 + \alpha_4 \eta \quad ; \quad \text{ie.} \quad \mathbf{A} = \begin{bmatrix} 1 & \eta & 0 & 0 \\ 0 & 0 & 1 & \xi \end{bmatrix} \end{aligned} \tag{41}$$

It is easy to check that the assumed shear strain field satisfies the inequalities (27) for meshes of more than 2×2 elements which guarantees the good behaviour of the element in practice.

The four α_i's are obtained by sampling the tangential shear strain $\gamma_{\bar{\xi}}$ of at the four points over the $\bar{\xi}$ directions shown in Figure 4. This gives

$$\underbrace{\begin{bmatrix} 1 & -1 & 0 & 0 \\ 0 & 0 & 1 & 1 \\ 1 & 1 & 0 & 0 \\ 0 & 0 & 1 & -1 \end{bmatrix}}_{\mathbf{P}} \begin{Bmatrix} \alpha_1 \\ \alpha_2 \\ \alpha_3 \\ \alpha_4 \end{Bmatrix} = \begin{Bmatrix} \gamma_{\bar{\xi}}^1 \\ \vdots \\ \gamma_{\bar{\xi}}^4 \end{Bmatrix} \quad \text{and} \quad \mathbf{P}^{-1} = \frac{1}{2} \begin{bmatrix} 1 & 0 & 1 & 0 \\ -1 & 0 & 1 & 0 \\ 0 & 1 & 0 & 1 \\ 0 & 1 & 0 & -1 \end{bmatrix} \tag{42}$$

The tangential shear strains $\gamma_{\bar{\xi}}^i$ are related with the $\gamma_\xi^i, \gamma_\eta^i$ by

$$\begin{Bmatrix} \gamma_{\bar{\xi}}^1 \\ \vdots \\ \gamma_{\bar{\xi}}^4 \end{Bmatrix} = \begin{bmatrix} 1 & 0 & & & & & & \mathbf{0} \\ & & 0 & 1 & & & & \\ & & & & 1 & 0 & & \\ \mathbf{0} & & & & & & 0 & 1 \end{bmatrix} \begin{Bmatrix} \gamma_\xi^1 \\ \gamma_\eta^1 \\ \vdots \\ \gamma_\xi^4 \\ \gamma_\eta^4 \end{Bmatrix} = \mathbf{T}\hat{\boldsymbol{\gamma}}^i \tag{43}$$

It is interesting to note that

$$[\mathbf{A}\ \mathbf{P}^{-1}\ \mathbf{T}] = \frac{1}{2} \left[\begin{array}{cccc|cccc} (1-\eta) & 0 & 0 & 0 & (1+\eta) & 0 & 0 & 0 \\ 0 & 0 & 0 & (1+\xi) & 0 & 0 & 0 & (1-\xi) \end{array}\right] \tag{44}$$

This expression could have been anticipated if the shear assumed strain field would have been directly written in the form

$$\begin{aligned} \gamma_\xi &= \frac{1}{2}(1-\eta)\gamma_\xi^1 + \frac{1}{2}(1+\eta)\gamma_\xi^3 \\ \gamma_\eta &= \frac{1}{2}(1+\xi)\gamma_\eta^2 + \frac{1}{2}(1-\xi)\gamma_\eta^4 \end{aligned} \tag{45a}$$

which gives

$$\begin{Bmatrix} \gamma_\xi \\ \gamma_\eta \end{Bmatrix} = [\mathbf{A}\ \mathbf{P}^{-1}\ \mathbf{T}] \begin{Bmatrix} \gamma_\xi^1 \\ \gamma_\eta^1 \\ \vdots \\ \gamma_\xi^4 \\ \gamma_\eta^4 \end{Bmatrix} \tag{45b}$$

from where the matrix product $\mathbf{A}\ \mathbf{P}^{-1}\ \mathbf{T}$ can be directly obtained.

The substitute shear strain matrix is finally obtained by eq.(37) with

$$\mathbf{C} = \begin{bmatrix} \mathbf{J}^1 & & & \mathbf{0} \\ & \mathbf{J}^2 & & \\ & & \mathbf{J}^3 & \\ \mathbf{0} & & & \mathbf{J}^4 \end{bmatrix} \quad \text{and} \quad \bar{\mathbf{B}}_s = \begin{Bmatrix} \mathbf{B}_s^1 \\ \vdots \\ \mathbf{B}_s^4 \end{Bmatrix} \tag{46}$$

For further reference this element will be termed QLLL (refering to Quadrilateral, biLinear deflections, biLinear rotations and Linear shear)

7.1 Nine node quadrilateral plate element with quadratic shear field

This element was originally presented by Hinton and Huang [10] and Bathe et al. [4]. From the expressions of the standard quadratic shape functions for ω and $\boldsymbol{\theta}$ [19] and the arguments of previous sections the following "correct" quadratic shear field can be obtained

$$\begin{aligned} \gamma_\xi &= \alpha_1 + \alpha_2\xi + \alpha_3\eta + \alpha_4\xi\eta + \alpha_5\eta^2 + \alpha_6\xi\eta^2 \\ \gamma_\eta &= \alpha_7 + \alpha_8\xi + \alpha_9\eta + \alpha_{10}\xi\eta + \alpha_{11}\xi^2 + \alpha_{12}\eta\xi^2 \end{aligned} \tag{47}$$

It can be checked that this element satisfies the conditions (27) for all element patches.

Figure 4 shows the 12 sampling points for computation of the α_i's. The derivation of matrix $\hat{\mathbf{B}}_s$ follows the steps given in previous section.

The computations can be simplied if the matrix product $\mathbf{A}\ \mathbf{P}^{-1}\ \mathbf{T}$ is directly obtained by writting eqs.(45) as

$$\begin{aligned} \gamma_\xi = &\frac{1}{4}[A\gamma_{\xi^1} + B\gamma_\xi^2]\eta(1+\eta) + \frac{1}{2}[A\gamma_\xi^3 + B\gamma_\xi^4](1-\eta^2)] + \\ &+ \frac{1}{4}[A\gamma_\xi^5 + B\gamma_\xi^6]\eta(\eta-1) \end{aligned} \tag{48}$$

with $A = 1+\sqrt{3}\xi$ and $B = 1-\sqrt{3}\xi$. A similar expression can be written for γ_η simply interchanging ξ by η and points 1 to 6 by 7 to 12, respectively. From (48) the matrix product $\mathbf{A}\ \mathbf{P}^{-1}\ \mathbf{T}$ is obtained as

$$\underset{2\times 24}{\mathbf{A}\ \mathbf{P}^{-1}\ \mathbf{T}} = \begin{bmatrix} \frac{A\eta_1}{4}, & 0, & \frac{B\eta_1}{4}, & 0, & \frac{A\eta_2}{2}, & 0, & \frac{B\eta_2}{2}, & 0, & \frac{A\eta_3}{4}, & 0, & \frac{B\eta_3}{4}, & 0, & \overset{0}{1\times 12} \\ \overset{0}{1\times 12}, & 0, & \frac{\bar{A}\xi_1}{4}, & 0, & \frac{\bar{B}\xi_1}{4}, & 0, & \frac{\bar{A}\xi_2}{4}, & 0, & \frac{\bar{B}\xi_2}{2}, & 0, & \frac{\bar{A}\xi_3}{2}, & 0, & \frac{\bar{B}\xi_3}{4} \end{bmatrix} \tag{49}$$

with $\bar{A} = 1+\sqrt{3}\eta$ $\bar{B} = 1-\sqrt{3}\eta$; $s_1 = s(1+s)$, $s_2 = 1-s^2$, $s_3 = s(s-1)$, $s = \xi, \eta$

The remaining $\mathbf{C}$ and $\bar{\mathbf{B}}_s$ matrices necesaries for computation of $\hat{\mathbf{B}}_s$ by eq.(37) are given by

$$\mathbf{C} = \begin{bmatrix} \mathbf{J}_1 & & \mathbf{0} \\ & \ddots & \\ \mathbf{0} & & \mathbf{J}_{12} \end{bmatrix} \quad , \quad \bar{\mathbf{B}}_s = \begin{Bmatrix} \mathbf{B}_s^1 \\ \vdots \\ \mathbf{B}_s^{12} \end{Bmatrix} \tag{50}$$

The same ideas can be used for obtaining the shear strain matrix of the eight node and other higher order quadrilateral plate elements. Details of the adequate shear constrained fields for some of these elements can be found in [10].

For further reference we will denote this element as QQQQ (Quadrilateral, Quadratic deflections, Quadratic rotations and Quadratic shears)

7.3 Six node quadratic triangular plate element with linear shear strain field

Recently [15], [24] the authors have shown the good performance of the six node triangular element with quadratic variations for both the deflection and the rotation fields and a linear interpolation of the shear strain (here termed TQQL for Triangular, Quadratic w, Quadratic $\boldsymbol{\theta}$ and Linear $\boldsymbol{\gamma}$) as

$$\begin{aligned} \gamma_\xi &= \alpha_1 + \alpha_2\xi + \alpha_3\eta \\ \gamma_\eta &= \alpha_4 + \alpha_5\xi + \alpha_6\eta \end{aligned} \quad ; \quad \mathbf{A} = \begin{bmatrix} 1 & \xi & \eta & 0 & 0 & 0 \\ 0 & 0 & 0 & 1 & \xi & \eta \end{bmatrix} \tag{51}$$

The location of the six shear sampling points is shown in Figure 4. It easy to check that the element passes satisfactionaly the conditions (27) for all element patches [21],[24].

The local directions $\bar{\xi}_i$ are shown in Figure 5. It can be easily found for this case

$$\mathbf{P} = \begin{bmatrix} 1 & \xi_1 & \eta_1 & 0 & 0 & 0 \\ 1 & \xi_2 & \eta_2 & 0 & 0 & 0 \\ -a & -a\xi_3 & -a\eta_3 & a & a\xi_3 & a\eta_3 \\ -a & -a\xi_4 & -a\eta_4 & a & a\xi_4 & a\eta_4 \\ 0 & 0 & 0 & 1 & \xi_5 & \eta_5 \\ 0 & 0 & 0 & 1 & \xi_6 & \eta_6 \end{bmatrix} \quad ; \quad \mathbf{T} = \begin{bmatrix} 1 & 0 & & & & & & & & & & \mathbf{0} \\ & & 1 & 0 & & & & & & & & \\ & & & & -a & a & & & & & & \\ & & & & & & -a & a & & & & \\ & & & & & & & & 0 & 1 & & \\ & \mathbf{0} & & & & & & & & & 0 & 1 \end{bmatrix}$$

$$\mathbf{C} = \begin{bmatrix} \mathbf{J}^1 & & & & & \mathbf{0} \\ & \mathbf{J}^2 & & & & \\ & & \mathbf{J}^3 & & & \\ & & & \mathbf{J}^4 & & \\ & & & & \mathbf{J}^5 & \\ & \mathbf{0} & & & & \mathbf{J}^6 \end{bmatrix} \quad , \quad \bar{\mathbf{B}}_s = \begin{Bmatrix} \mathbf{B}_s^1 \\ \mathbf{B}_s^2 \\ \vdots \\ \mathbf{B}_s^6 \end{Bmatrix} \quad , \quad a = \frac{\sqrt{2}}{2} \tag{52}$$

From eqs.(51) and (52) the substitute shear strain matrix of eq.(37) can be readily obtained.

It has been checked that this element behaves well and it converges to the exact solution in all examples analyzed [15], [24]. However, for coarse meshes its behaviour is too flexible. A way to reduce the flexibility of the element, still preserving satisfaction of eqs.(27) is to eliminate the normal rotations at the mid-side nodes. This can be simply done by introducing the constraint $\theta_n^i - \frac{1}{2}(\theta_n^{i-1} + \theta_n^{n+1}) = 0$ in a penalized manner into the expression of the total potential energy (5) as

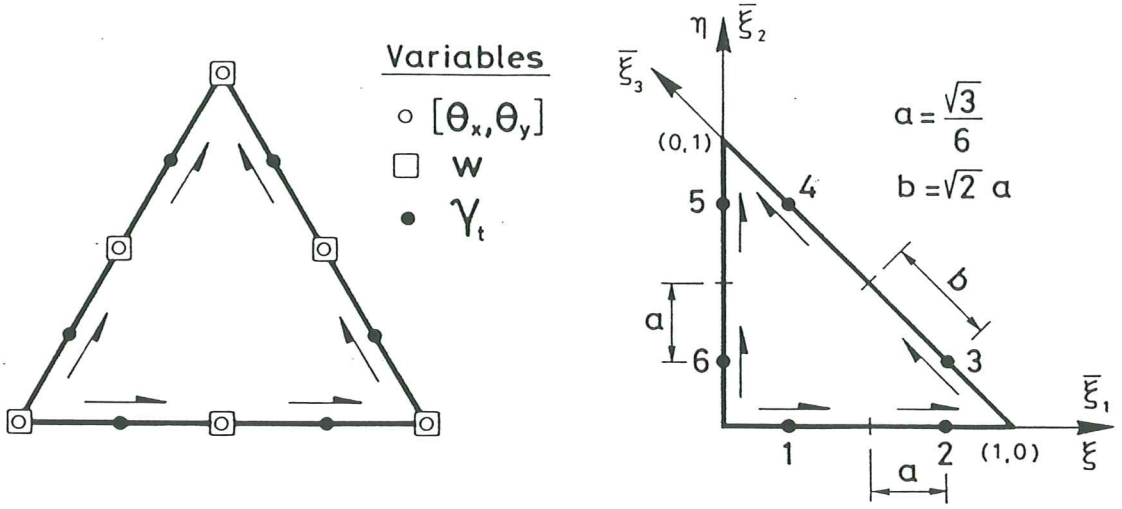

Figure 5. Six node quadratic triangular plate element with linear shear strain field (TQQL).

$$\bar{\Pi} = \Pi + \frac{\beta}{2}\left[\theta_n^i - \frac{1}{2}(\theta_n^{i-1} + \theta_n^{i+1})\right]^2 \tag{53}$$

where β is an appropiate penalty parameter. Numerical experience has shown that $\alpha = 10^3 Gt$ suffices to obtain good results.

A method of imposing this constraint explicity is given in next section.

7.4 Linear/Quadratic triangle

An improved version of the quadratic triangle of the preceeding section, also presented by the authors in [15] and [24], is the following:

1) The deflection w varies linearly over the element as

$$w = \sum_{i=1}^{3} L_i \bar{w}_i \tag{54}$$

2) An incomplete quadratic variation of the rotations within the element is obtained according to the following interpolation

$$\boldsymbol{\theta} = \sum_{i=1}^{3} L_i \bar{\boldsymbol{\theta}}_i + 4\, L_1 L_2 \mathbf{e}_{12} \Delta\theta_{t_4} + 4 L_2 L_3 \mathbf{e}_{23} \Delta\theta_{t_5} + 4 L_3 L_1 \mathbf{e}_{13} \Delta\theta_{t_6} \tag{55}$$

where L_i are the standard linear shape functions of the three node triangle, $\Delta\theta_{t_k}$ is a hierarchical tangential rotation parameter at the element mid-side and $\mathbf{e}_{ij}$ is an unit vector indicating the direction of the element sides (Figure 6).

The vector of nodal variables can be written as

$$\bar{\mathbf{u}}_i = [w_1, \theta_{x_1}, \theta_{y_1}, w_2, \theta_{x_2}, \theta_{y_3}, w_3, \theta_{x_3}, \theta_{y_3}, \Delta\theta_{t_4}, \Delta\theta_{t_5}, \Delta\theta_{t_6}]^T \tag{56}$$

3) The shear strain field is again assumed to be linear in each element but the tangential shear strains are assumed *constant* along each side.

From eq.(55) it can be deduced that the normal rotation varies linearly along the sides, whereas the tangential rotation varies quadratically over the element.

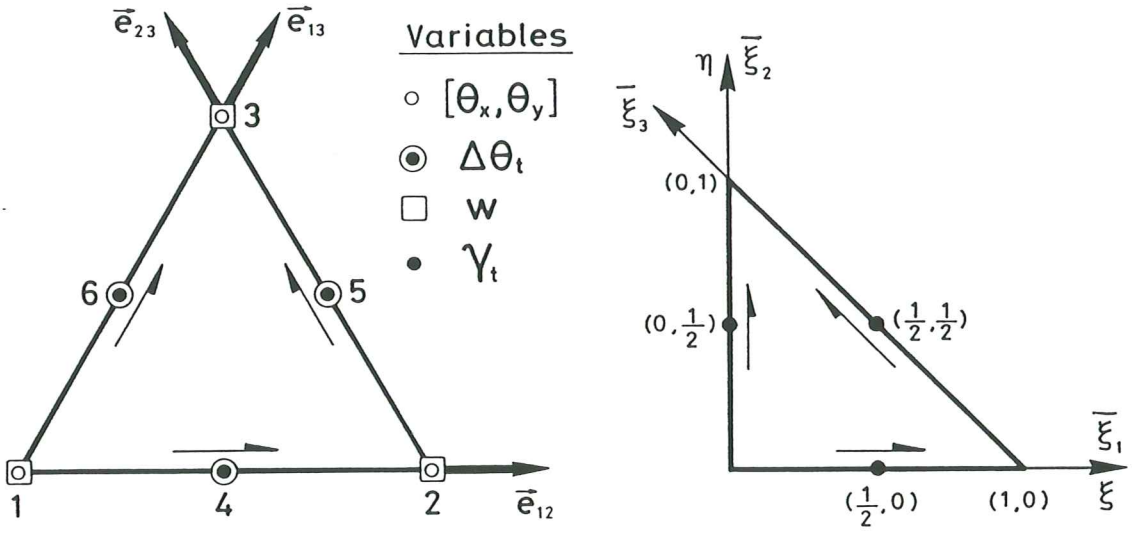

Figure 6. TLQL triangular element (linear w, quadratic $\mathbf{q}$ and linear shear).

It can also be verified that the element satisfies condition (27) for all patches.

The derivation of the substitute shear strain for this element, DRM in [24] and TLQL hereafter (for **T**riangular, **L**inear w **Q**uadratic $\boldsymbol{\theta}$ and **L**inear $\boldsymbol{\gamma}$), is simple if we start from the six points strain field of the quadratic triangle of Figure 6. This immediately gives matrices $\mathbf{A}$ and $\mathbf{P}$ identicals to those of eqs.(51) and (52), respectively. Condition (3) is now accomplished by setting $\gamma_{\bar{\xi}}^1 = \gamma_{\bar{\xi}}^2 = \gamma_{\bar{\xi}}^{12}$, $\gamma_{\bar{\xi}}^3 = \gamma_{\bar{\xi}}^4 = \gamma_{\bar{\xi}}^{23}$ and $\gamma_{\bar{\xi}}^5 = \gamma_{\bar{\xi}}^6 = \gamma_{\bar{\xi}}^{13}$, which yields the following matrix expression

$$\begin{Bmatrix} \gamma_{\bar{\xi}}^{1} \\ \gamma_{\bar{\xi}}^{2} \\ \vdots \\ \gamma_{\bar{\xi}}^{6} \end{Bmatrix} = \begin{bmatrix} 1 & 0 & & & & \mathbf{0} \\ 1 & 0 & & & & \\ & & 1 & 0 & & \\ & & 1 & 0 & & \\ & & & & 0 & 1 \\ \mathbf{0} & & & & 0 & 1 \end{bmatrix} \begin{Bmatrix} \gamma_{\bar{\xi}}^{12} \\ \gamma_{\bar{\xi}}^{23} \\ \gamma_{\bar{\xi}}^{13} \end{Bmatrix} = \mathbf{T}\hat{\boldsymbol{\gamma}}' \tag{57}$$

where $\gamma_{\bar{\xi}}^{ij}$ denotes the constant tangential natural shear strain along the element side ij. The value of $\gamma_{\bar{\xi}}^{ij}$ for each side is obtained from eq.(38) with $W = 1$ (Galerkin) as

$$\gamma_{\bar{\xi}}^{ij} = \frac{1}{l_{\bar{\xi}}^{ij}} \int_{l_{\bar{\xi}}} \left(\frac{\partial w}{\partial \bar{\xi}} + \theta_{\bar{\xi}} \right) d\bar{\xi} = \pm \frac{1}{l_{\bar{\xi}}^{ij}} (w_j - w_i) +$$

$$+ \frac{1}{2} \mathbf{e}_{ij}^{T} (\boldsymbol{\theta}_i + \boldsymbol{\theta}_j) \frac{l^{ij}}{l_{\bar{\xi}}^{ij}} + \frac{2}{3} \Delta\theta_{t_k} \frac{l^{ij}}{l_{\bar{\xi}}^{ij}} \tag{58}$$

where $k = 3 + i$, l^{ij} is the *actual* lenght of the element side, $l_{\bar{\xi}}^{12} = l_{\bar{\xi}}^{13} = 1$ and $l_{\bar{\xi}}^{23} = \sqrt{2}$. The $\pm$ ambiguity in (58) is due to the fact that the direction of the tangential shear must be defined by an unique direction on each edge of contiguous elements. Failure to achieve this results in an inconsistent definition of the edge incremental rotation degree of freedom $\Delta\theta_{t_k}$. A way to overcome this dificulty is to define the direction for $\mathbf{e}_{ij}$ in the direction of increasing (global) node numbers for the end points of each element edge. The sign in (58) is chosen to be positive if the direction of $\mathbf{e}_{ij}$ corresponds to that for constructing the boundary integrals, otherwise a negative sign is inserted.

Eqs.(57) and (58) allow to obtain an explicit form between the tangential natural shear strains and the nodal displacements as

$$\boldsymbol{\gamma}_{\bar{\xi}} = \mathbf{T}[CB]\bar{\mathbf{u}} = [TCB]\bar{\mathbf{u}} \tag{59}$$

where $\mathbf{T}$ is defined by eq.(57) and

$$[CB] = \begin{bmatrix} \mp 1, & \frac{C_{12}l^{12}}{2}, & \frac{S_{12}l^{12}}{2}, & \pm 1, & \frac{C_{12}l^{12}}{2}, & \frac{S_{12}l^{12}}{2}, & 0, & 0, & 0, & \frac{2}{3}l^{12}, & 0, & 0 \\ 0, & 0, & 0, & \frac{\mp 1}{\sqrt{2}}, & \frac{C_{23}l^{23}}{2\sqrt{2}}, & \frac{S_{23}l^{23}}{2\sqrt{2}}, & \frac{\pm 1}{\sqrt{2}}, & \frac{C_{23}l^{23}}{2\sqrt{2}}, & \frac{S_{23}l^{23}}{2\sqrt{2}}, & 0, & \frac{\sqrt{2}}{3}l^{23}, & 0 \\ \pm 1, & \frac{C_{13}l^{13}}{2}, & \frac{S_{13}l^{23}}{2}, & 0, & 0, & 0, & \mp 1, & \frac{C_{13}l^{13}}{2}, & \frac{S_{13}l^{13}}{2}, & 0, & 0, & \frac{2}{3}l^{13} \end{bmatrix} \tag{60}$$

where S_{ij}, C_{ij} are the components of the side unit vector $\mathbf{e}_{ij} = [C_{ij}, S_{ij}]^T$ of Figure 6.

The substitute shear strain matrix for the TLQL element can now be readily obtained by eq.(40).

REMARK 3

Obviously the choice of $W = 1$ in eq.(38) yielding the relation (58) between the constant shear strain along each side and the nodal displacements is not the only possible one. Many other option for the weighting of eq. (38) can be attempted (point collocation, subdomain collocation, etc.) each one yielding a different element. a study of the numerical benefit of the diferent alternatives for selecting W is currently investigated by the authors.

REMARK 4

The hierarchical rotation $\Delta\theta_{t_k}$ can be eliminated by imposing the vanishing of the shear strain $\gamma_{\bar{\xi}}^{ij}$ along each side. This gives

$$\gamma_{\bar{\xi}}^{ij} = 0 \Rightarrow \Delta\theta_{t_k} = \frac{\mp 3}{2l^{ij}}(w_j - w_i) - \frac{3}{4}\mathbf{e}_{ij}^T(\boldsymbol{\theta}_i + \boldsymbol{\theta}_j) \tag{61}$$

It is interesting to note that the resulting rotation field is identical to that of the standard three node DKT element of Batoz et al. [5], this yielding the same stiffness matrix in both cases.

7.5 Bilinear/quadratic quadrilateral with linear shear strain field

The above ideas can be easily applied to derive a new quadrilateral element with the following displacement and shear strain fields:

(1) The deflection w varies bilinearly over the element as

$$w = \sum_{i=1}^{4} N_i w_i \tag{62}$$

where N_i are the standard bilinear shape functions of the C° four node rectangle.

(2) An incomplete quadratic variation of the rotation is chosen as

$$\boldsymbol{\theta} = \sum_{i=1}^{4} N_i \bar{\boldsymbol{\theta}}_i + f(\xi)(1-\eta)\mathbf{e}_{12}\Delta\theta_{t_5} + f(\eta)(1+\xi)\mathbf{e}_{23}\Delta\theta_{t_6} +$$

$$+ f(\xi)(1+\eta)\mathbf{e}_{43}\Delta\theta_{t_7} + f(\eta)(1-\xi)\mathbf{e}_{14}\Delta\theta_{t_8} \tag{63}$$

with $f(\xi) = 1 - \xi^2$ y $f(\eta) = 1 - \eta^2$.

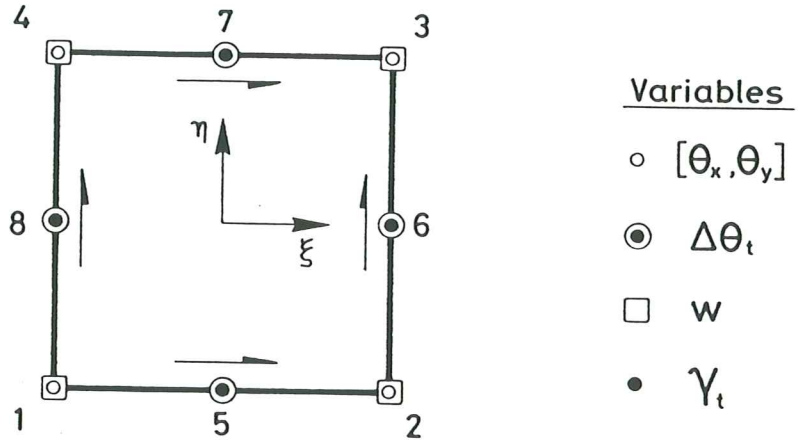

Figure 7. QLQL quadrilateral plate element (linear w, quadratic θ and linear shear.)

(3) The shear strain field is assumed to be linear in each element and equal to that of eq.(41).

It is easy to check that this element termed QLQL (Figure 7) satisfies conditions (17) for all element patches.

The derivation of the substitute shear strain matrix for the QLQL element follows precisely the steps explained in eqs.(41)–(46) for the standard four node cuadrilateral (QLLL).

It is interesting to note that an elimination of the hierarchical tangential rotation along the sides by an equation similar to (61) will yield a four node Discrete Kirchoff Cuadrilateral similar to that presented by Batoz and Tahor [6].

8. NUMERICAL EXAMPLES

The behaviour of the different elements has been tested in the analysis of thick and thin simply supported (SS) and fully clamped (CL) square plates under an uniform loading q and a central point load P. The structural properties of the plate are $E = 10.92$, $\nu = 0.3$, side length$= 10$. The intensity of the loadings are $q = 1.0$ and $p = 1.0$. Hard ($w = \theta_s = 0$) boundary conditions have been assumed for the SS case.

Figures 8 and 9 show the convergence of the central deflection versus the total number of degrees of freedom for the TLQL triangular element of section 7.4, for different thicknesses ($a/t = 10$ to 10^6), mesh orientations and boundary condition for the uniform loading and central point loading, respectively. Note: (a) The excellent convergence of the element for all the range of thickness considered for both the SS and CL cases. (b) The sensitivity of the solution to the mesh orientation.

Figure 10 compares the error in the central displacement versus the total numbers of degrees of freedom for the TQQL and TLQL triangular elements for the SS case, uniform loading and thick and thin conditions. Results show the greater efficiency of the TLQL element. Further evidence of the excellent behaviour of this element can be found in [15] and [24].

Figure 11 shows the convergence of the center displacement for the QLQL quadrilateral element for the same plate cases previously analyzed. Again excellent convergence for all cases is obtained. Figure 12 compares the convergence of the QLLL, QQQQ and QLQL quadrilateral elements under uniform loading for the SS case and thick and thin plate situations. It can be seen the big efficiency of the QLQL element for the case studied.

Finally, the convergence of the new QLQL quadrilateral and the TLQL triangular elements is compared in Figure 13, again for uniform loading, SS conditions and thick and thin situations. Both elements show excellent convergence in all cases and less than 0.5% error is always obtained with meshes of just over 10 degrees of freedom

9. CONCLUSIONS

In the paper we have shown that the condition of vanishing shear strains for the thin plate limit imposes that the coefficients defining the shear strains polynomial field must be a linear function of the nodal rotations and deflections. This explains the success of reduced integration techniques and the use of substitute transverse shear strain fields which satisfy that condition. Indeed as discussed in [19] this shows why the so called discrete Kirchhoff constraints are an efficent way of designing this plate elements. A general expression for the substitute shear strain matrix has been obtained which can be useful for the practical derivation of shear constrained elements based on adequate shear /displacement fields. This methodology has been applied to some of the existing plate elements and, in particular, to the new TLQL triangular and QLQL quadrilateral elements which show an excellent behaviour for thick and thin plate analysis. The possibilities of the methodology presented for deriving new discrete Kirchhoff elements have also been outlined and this opens a line for future research in this field

REFERENCES

1. S. Ahmad, B.M. Irons and O.C. Zienkiewicz, "Analysis of thick and thin shell structures by curved finite elements", *Int. J. Numer. Meth. Eng.*, **2**, 419–451, 1970.
2. D.N. Arnold and S.N. Falk, "A uniform formuly accurate finite element method for the Mindlin-Reissner plate", Preprint 307, Inst. for Mathematics and its Applicat., Univ. of Minnesota, 1987.
3. K.J. Bathe and E.N. Dvorkin, "A four node plate bending element based on Mindlin/Reissner plate theory and mixed interpolation", *Int. J. Numer. Meth. Eng.*, **21**, 367–383, 1985.
4. K.J. Bathe, F. Brezzi and S. Cho. The MITC7 and MITC9 plate bending elements, *Comp. and Structures*, **32**, 3–4, 797–814, 1989.
5. J.L., Batoz, K.J. Bathe and L.W. Ho, "A study of three node triangular plate bending elements, *Int. J. Num. Meth. engng.*, **15**, 1771–812, 1980.
6. J.L. Batoz and M.B. Tahor, "Evaluation of a new quadrilateral thin plate bending element", *Int. J. Num. Meth. Engng.*, **18**, 1655–77, 1982.
7. F. Brezzi, K.J. Bathe and M. Fortun, " Mixed interpolation for Reissner-Mindlin plates", *Int. J. Num. Meth. Engng.*, **28**, 1787-801, 1989.
8. M.A. Crisfield, "A four-noded thin-plate bending element using shear constrains-A modified version of Lyon's element", *Comp Meth. Appl. Mech. Eng.*, **38**, 93–120, 1983.
9. E.N. Dvorkin and K.J. Bathe, "A continuum mechanics based four node shell element for general non-linear analysis", *Eng. Comp.*, **1**, 77–88, 1984.
10. E. Hinton and H.C. Huang, "A family of quadrilateral Mindlin plate element with substitute shear strain fiels", *Comp. and Struct.*, **23**, 409–431, 1986.
11. T.J.R. Hughes, R.L. Taylor and W. Kanoknukulchai, "A simple and efficient element for plate bending", *Int. J. Numer Meth. Eng.*, **11**, 1529–1543, 1977.
12. T.J.R. Hughes, L.Taylor and T.E. Tezduyar, "Finite elements based upon Mindlin plate theory with particular reference to the four node bilinear isoparametric element", *J. Appl. Mech.*, **46**, 587–596, 1981.
13. D.S. Malkus and T.J. R. Hughes, "Mixed finite element methods-reduced and selective intergration techniques: A unification of concepts, *Comp. Meth. Appl. Mech. Eng.* , **15** 63–81, 1978.
14. R.D. Mindlin, "Influence of rotatory inertia and shear in flexural motions of isotropic elastic plates", *J. Appl. Mech.*, **18**, 31–38, 1951.
15. E.Oñate, R.L. Taylor and O.C. Zienkiewicz, "Consistent formulation of shear constrained Reissner-Mindlin plate elements", in *Discretization Methods in Structural Mechanics*, G. Kuhn and H. Mang (Eds.), Springer-Verlag, 1990.
16. E.D.L. Pugh, E. Hinton and O.C. Zienkiewicz, "A Study of Quadrilateral plate bending elements with reduced integration", *J. Appl. Mech.*, **12**, 1059-1079, 1978.
17. E. Reissner, "The effect of transverse shear deformation on the bending of elastic plates, *J. Appl. Mech.*, **12** 69–76, 1945.
18. S. Timoshenko and S. Woinowsky-Krieger, *Theory of Plates and Shells*, Mc Graw-Hill, 1959.
19. O.C. Zienkiewicz and R.L. Taylor, *The Finite Element Method* , 4d Edition, Mcgraw Hill, London, 1991.

20. O.C. Zienkiewicz and D. Lefebvre, "Three field mixed approximation and the plate bending problem", *Comm. Appl. Numer. Meth.*, **3** 301–309, 1987.
21. O.C. Zienkiewicz and D. Lefebvre, " A robust triangular plate bending element of the Reissner-Mindlin type", *Int. J. Numer Meth. Eng.*, **26**, 1169-1184, 1988.
22. O.C. Zienkiewicz , J. Too and R.L. Taylor, "Reduced integration techniques in general analysis of plates and shells", *Int. J. Numer Meth. Eng.*, **3**, 275–290, 1971.
23. O.C. Zienkiewicz, S. Qu, R.L. Taylor and S. Nakazawa, "The Patch test for mixed formulations", *Int. J. Numer Meth. Eng.*, **23**, 1873–1883, 1986.
24. O.C. Zienkiewicz, R.L. Taylor, P. Papadopoulus and E. Oñate, "Plate bending elements with discrete constraints: New Triangular Elements", *Comp. and Struct.*, **35**, 4, 505–22, 1990.

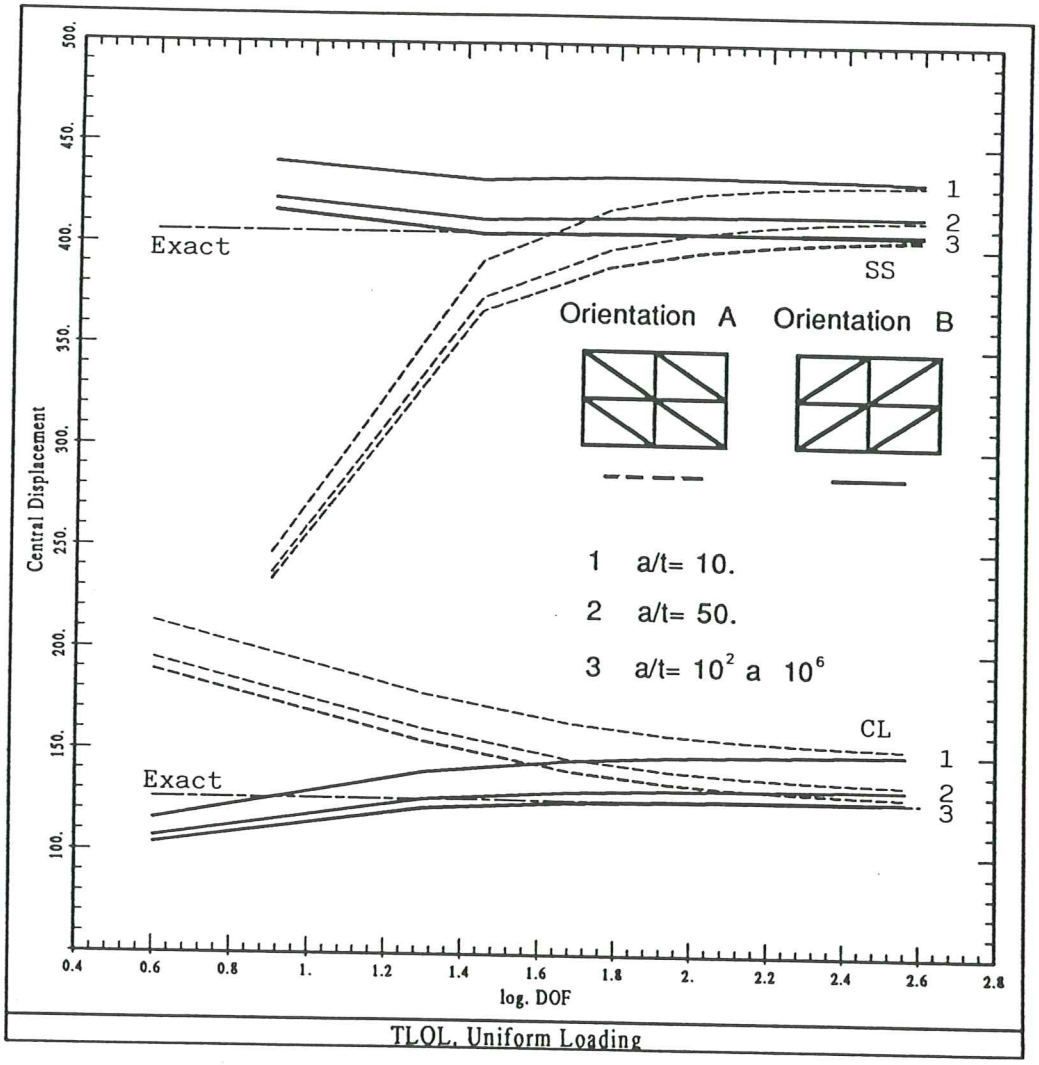

Figure 8. TLQL triangular plate element. Convergence of central deflection with degrees of freedom for simply supported (SS) and clamped (CL) square plates under uniform loading for different thicknesses and mesh orientations. Exact solutions obtained from [18].

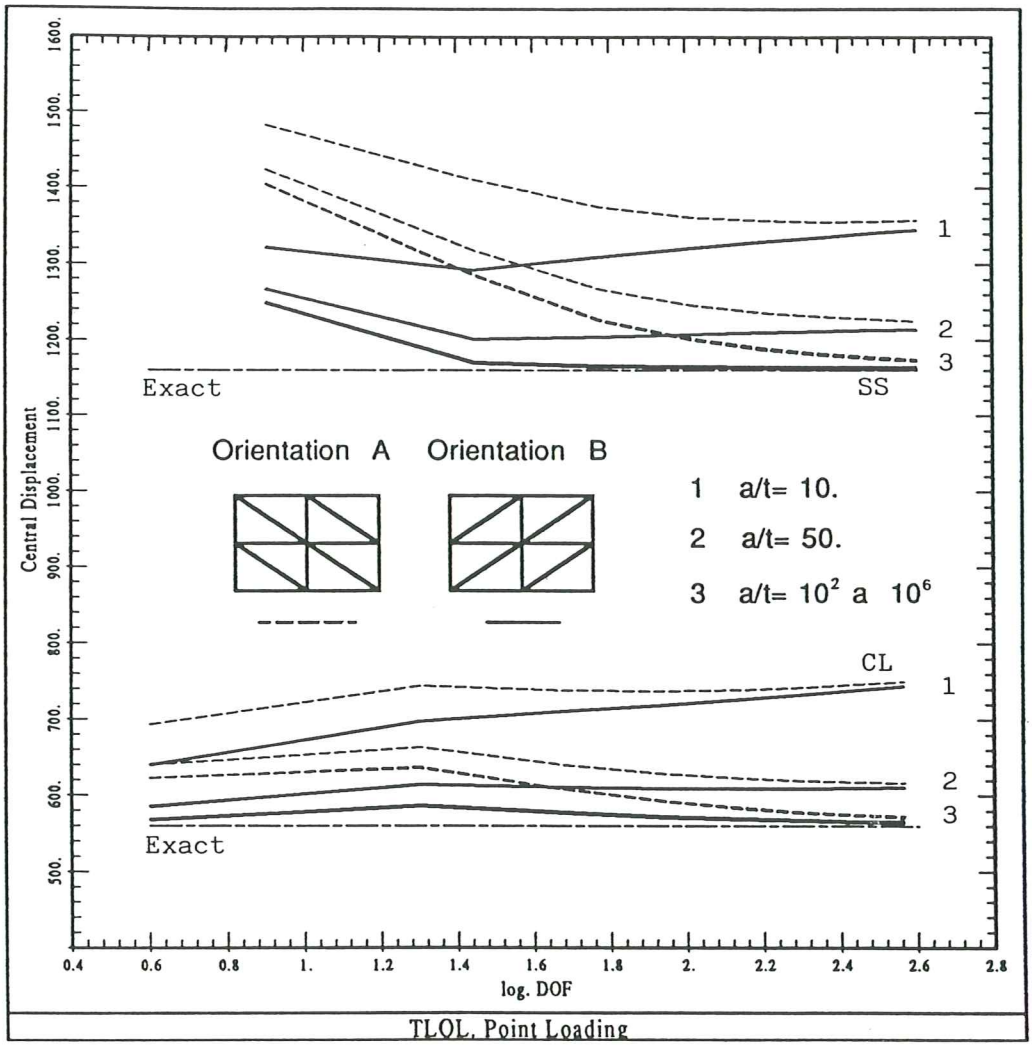

Figure 9. TLQL triangular plate element. Convergence of central deflection with degrees of freedom for simply supported (SS) and clamped (CL) square plates under central point loading for different thicknesses and mesh orientations. Exact solutions obtained from [18].

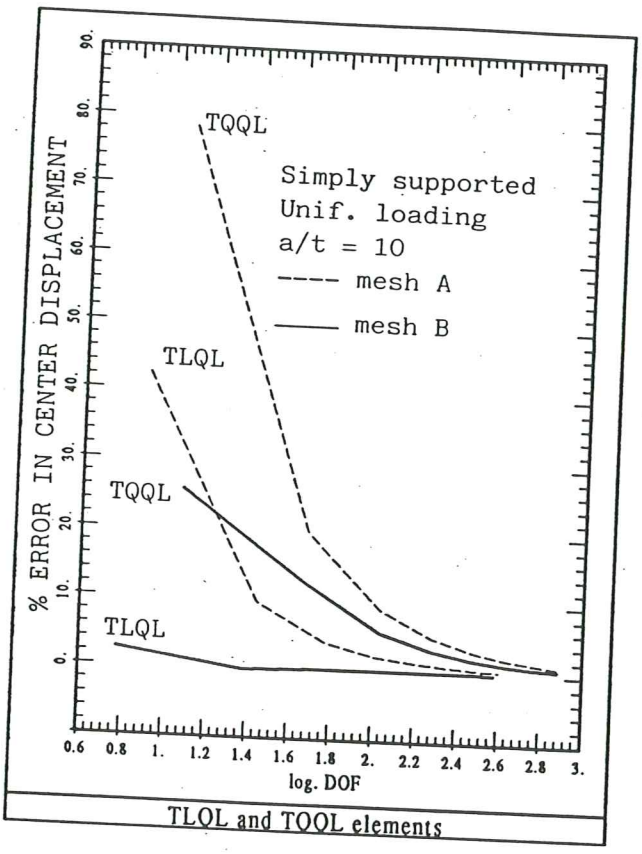

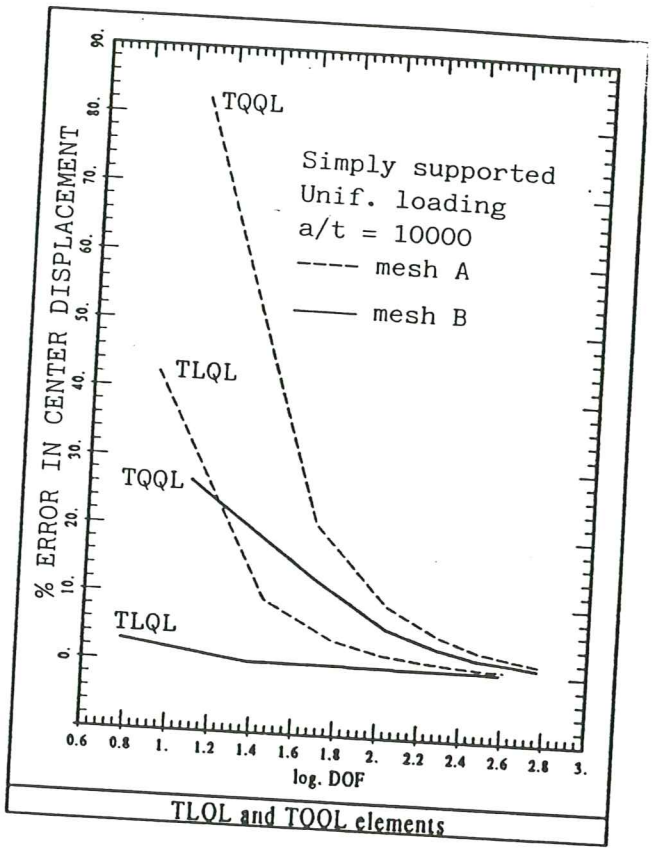

Figure 10. Simply supported square plate under uniform loading. Error in center displacement versus degrees of freedom for TLQL and TQQL triangular elements for different thicknesses ($a/t = 10$ and $a/t = 1000$) and mesh orientations.

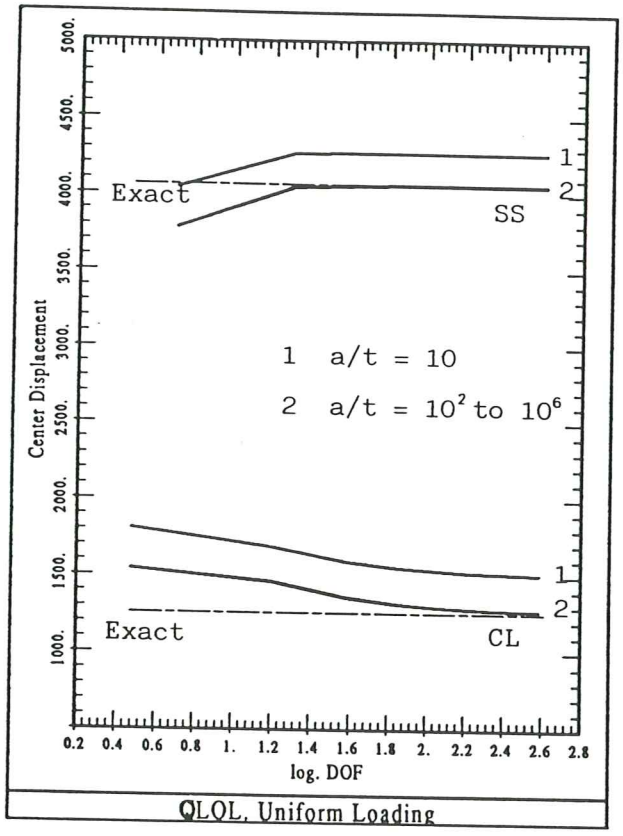

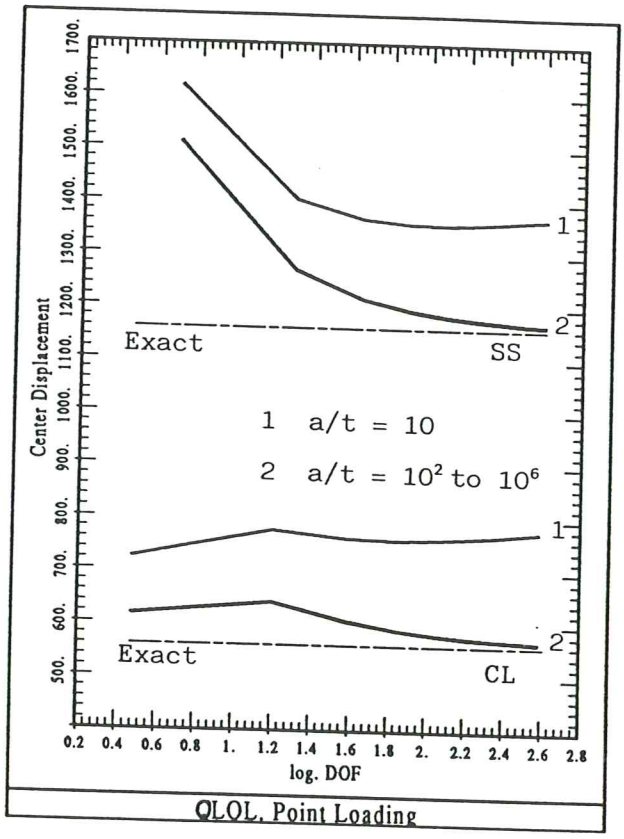

Figure 11. QLQL quadrilateral plate element. Convergence of center displacement with number of degrees of freedom for simply supported (SS) and clamped (CL) square plates under uniform loading and central point loading for different thicknesses. Exact solutions obtained from [18].

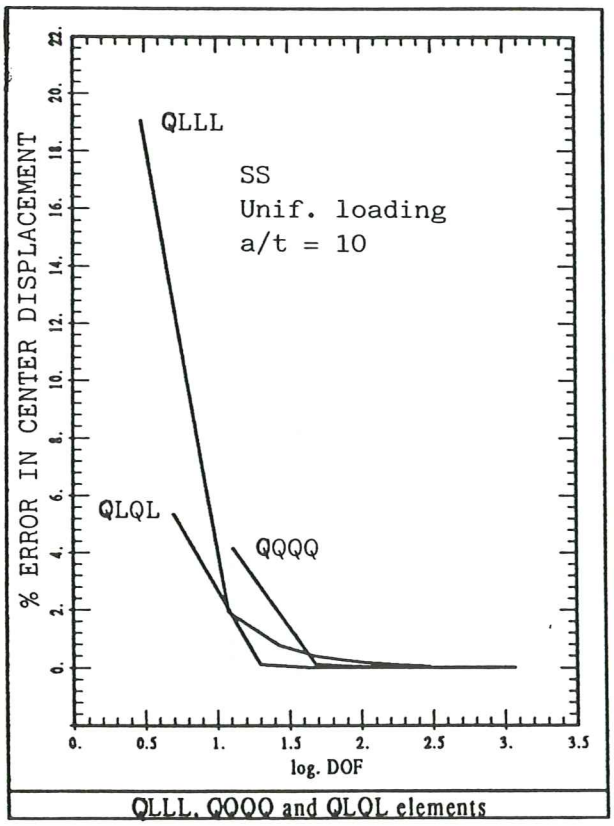

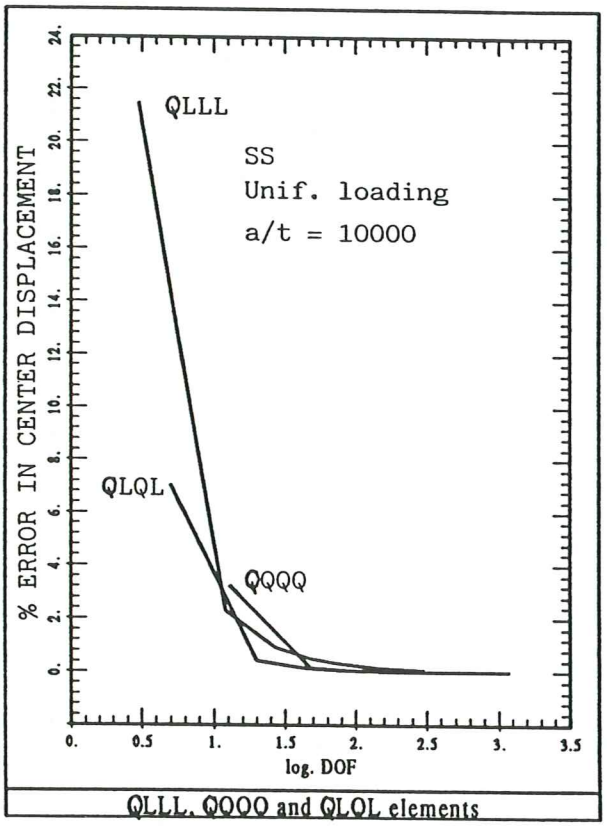

Figure 12. Simply supported square plate under uniform loading. Error in center displacement versus degrees of freedom for QLLL, QQQQ and QLQL quadrilateral elements for thick ($t/l = 10$) and thin ($t/l = 1000$) situations.

APPENDIX A. PROOF OF THE SINGULARITY RULE FOR $\mathbf{K}_s$.

Let's write the substitute shear strain of eq.(37) for the whole mesh as

$$\underset{2\times n}{\hat{\mathbf{B}}_s} = \underset{2\times 2}{\mathbf{J}^{-1}}\ \underset{2\times n_\gamma}{\mathbf{A}}\ \underset{n_\gamma\times n_\gamma}{\mathbf{P}^{-1}}\ \underset{n_\gamma\times 2n_\gamma}{\mathbf{T}}\ \underset{2n_\gamma\times n}{\begin{Bmatrix}\mathbf{B}_s^1\\ \vdots \\ \mathbf{B}_s^{n_\gamma}\end{Bmatrix}} = \underset{2\times n_\gamma}{[JAP]}\ \underset{n_\gamma\times n}{\begin{Bmatrix}\overset{\circ}{\mathbf{B}}{}_s^1\\ \vdots \\ \overset{\circ}{\mathbf{B}}{}_s^{n_\gamma}\end{Bmatrix}} = [JAP]\overset{\circ}{\mathbf{B}}_s \qquad (A.1)$$

$$\text{where}\quad [JAP] = \mathbf{J}^{-1}\,\mathbf{A}\,\mathbf{P}^{-1}\quad \text{and}\quad \underset{n_\gamma\times n}{\overset{\circ}{\mathbf{B}}_s} = \mathbf{T}\begin{Bmatrix}\mathbf{B}_s^1\\ \vdots \\ \mathbf{B}_s^{n_\gamma}\end{Bmatrix} \qquad (A.2)$$

In $(A.2)$ n_γ is the *total number* of constraints in the shear strains and n the number of nodal variables.

The shear stiffness matrix $\mathbf{K}_s$ is obtained from (13) with $\hat{\mathbf{B}}_s$ unstead of $\mathbf{B}_s$. Noting that $\overset{\circ}{\mathbf{B}}_s$ is constant over the element, we can write

$$\underset{n\times n}{\mathbf{K}_s} = \int\int_A \overset{\circ}{\mathbf{B}}_s[JAP]^T\,\mathbf{D}_s[JAP]\overset{\circ}{\mathbf{B}}_s dA =$$

$$= \overset{\circ}{\mathbf{B}}{}_s^T\left(\int\int_A \underset{n_\gamma\times 2}{[JAP]^T}\ \underset{2\times 2}{\mathbf{D}_s}\ \underset{2\times n_\gamma}{[JAP]}\,dA\right)\overset{\circ}{\mathbf{B}}_s = \underset{n\times n_\gamma}{\overset{\circ}{\mathbf{B}}{}_s^T}\ \underset{n_\gamma\times n_\gamma}{\overset{\circ}{\mathbf{D}}_s}\ \underset{n_\gamma\times n}{\overset{\circ}{\mathbf{B}}_s} \qquad (A.3)$$

The equilibrium equations for a node i can be written (taking into account the contribution from $\mathbf{K}_s$ only)

$$\mathbf{f}_i = \sum_{j=1}^{n}\mathbf{K}_{s_{ij}}\,\bar{\mathbf{u}}_j = \overset{\circ}{\mathbf{B}}{}_{s_i}^T\left[\overset{\circ}{\mathbf{D}}_s\,\overset{\circ}{\mathbf{B}}_{s_1}\bar{\mathbf{u}}_1 + \overset{\circ}{\mathbf{D}}_s\,\overset{\circ}{\mathbf{B}}_{s_2}\,\bar{\mathbf{u}}_2 + \cdots + \overset{\circ}{\mathbf{D}}_s\,\overset{\circ}{\mathbf{B}}_{s_n}\,\bar{\mathbf{u}}_n\right] \qquad (A.4)$$

From eq.$(A.4)$ we can deduce that if n_γ is the number of rows of $\overset{\circ}{\mathbf{B}}_{s_i}$ vector $\mathbf{f}_i$ is a combinations of n_γ linear relationships in $\bar{\mathbf{u}}_1, \bar{\mathbf{u}}_2, \cdots, \bar{\mathbf{u}}_n$. Hence, eq.$(A.4)$ can be rewritten afther eliminating the prescribed degrees of freedom, as

$$\begin{aligned}
&C_1^1(\alpha_1^1u_1+\cdots+\alpha_j^1u_j) + C_2^1(\alpha_1^2u_1+\cdots+\alpha_j^2u_j) + \cdots + C_{n_\gamma}^1(\alpha_1^ju_1+\cdots+\alpha_j^ju_j) = f_1\\
&C_1^2(\alpha_1^1u_1+\cdots+\alpha_j^1u_j) + C_2^2(\alpha_1^2u_1+\cdots+\alpha_j^2u_j) + \cdots + C_{n_\gamma}^2(\alpha_1^ju_1+\cdots+\alpha_j^ju_j) = f_2\\
&\qquad\vdots \qquad\qquad\qquad\vdots \qquad\qquad\qquad\vdots\\
&C_1^j(\alpha_1^1u_1+\cdots+\alpha_j^1u_j) + C_2^j(\alpha_1^2u_1+\cdots+\alpha_j^2u_j) + \cdots + C_{n_\gamma}^j(\alpha_1^ju_1+\cdots+\alpha_j^ju_j) = f_j
\end{aligned} \qquad (A.5)$$

where $j = n_\theta + n_\omega$ is the number of *free* degrees of freedom.

The system of equation $(A.5)$ will become singular of the coefficients $C_1^i, C_2^i, \cdots, C_{n_\gamma}^i$ of any of the above equations of the other rows, i.e. if we can solve

$$\begin{aligned} C_1^j &= B_1 C_1^1 + B_2 C_1^2 + \cdots + B_r C_1^r \\ C_2^j &= B_1 C_2^1 + B_2 C_2^2 + \cdots + B_r C_2^r \\ &\vdots \qquad\quad \vdots \qquad\qquad \vdots \\ C_{n_\gamma}^j &= B_1 C_{n_\gamma}^1 + B_2 C_{n_\gamma}^2 + \cdots + B_r C_{n_\gamma}^r \end{aligned} \tag{A.6}$$

with $r \leq j - 1$. The solution of $(A.6)$ is possible only if the number of coefficients, r, is greater or equal to the number of equation n_γ, i.e.

$$r \geq n_\gamma$$

or

$$j = n_\theta + n_\omega > n_\gamma$$

wich is the singularity condition for the solution of $(A.4)$.